

Real-Time Monitoring of Seismic Activity in the Kiskatinaw Area, Northeastern British Columbia (NTS 093P, 094A)

R.O. Salvage, University of Calgary, Calgary, Alberta, rebecca.salvage1@ucalgary.ca

J. Dettmer, University of Calgary, Calgary, Alberta

T.H.A. Swinscoe, University of Calgary, Calgary, Alberta

K. MacDougall, University of Calgary, Calgary, Alberta

D.W. Eaton, University of Calgary, Calgary, Alberta

M. Stacey, Nanometrics Seismic Monitoring Services, Ottawa, Ontario

M. Aboud, Nanometrics Seismic Monitoring Services, Ottawa, Ontario

T.-S. Kang, Pukyong National University, Busan, South Korea

S. Kim, Chungnam National University, Daejeon, South Korea

J. Rhie, Seoul National University, Seoul, South Korea

Salvage, R.O., Dettmer, J., Swinscoe, T.H.A., MacDougall, K., Eaton, D.W., Stacey, M., Aboud, M., Kang, T.-S., Kim, S. and Rhie, J. (2021): Real-time monitoring of seismic activity in the Kiskatinaw area, northeastern British Columbia (NTS 093P, 094A); *in* Geoscience BC Summary of Activities 2020: Energy and Water, Geoscience BC, Report 2021-02, p. 17–30.

Introduction

Over the past decade, hydraulic fracturing and wastewater disposal operations have significantly increased in the Western Canada Sedimentary Basin (WCSB) due to development of a number of distinct resource plays, including the Montney. Due to the temporal and spatial correlation of increased seismicity with increased operations in this area, this trend is generally attributed to anthropogenic causes, although very few hydraulic fracturing operations (0.3%) are actually linked to seismic activity with moment magnitudes (M_w) >3 (Rivard et al., 2014; Atkinson et al., 2016). In recent years, northeastern British Columbia (BC) has experienced an increasing number of felt seismic events during active development within the Montney play. This led the British Columbia Oil and Gas Commission (BCOGC) to implement a special order in 2018 (BC Oil and Gas Commission, 2018) within the area now known as the Kiskatinaw Seismic Monitoring and Mitigation Area (KSMMA; Figure 1). This order required operators to undertake a pre-assessment of the seismic hazard, fully inform residents in the area of upcoming operations and monitor seismic activity in real-time before, during and after completions. Of particular importance was the introduction within the KSMMA of the cessation of operations following an event with a local magnitude (M_L) of ≥ 3.0 (BC Oil

and Gas Commission, 2018), which is lower than the M_L 4.0 threshold that is standard elsewhere in BC (e.g., Babaie Mahani and Kao, 2020).

Although the KSMMA is heavily monitored for seismic activity by individual companies undertaking resource development, limited real-time public data were available to better understand exactly how and why this area is so susceptible to induced seismicity, how faults are activated during hydraulic fracturing operations and why low magnitude events ($M_L < 2$) are often felt by residents. Although a number of larger felt events have occurred within the KSMMA (e.g., November 30, 2018, near Fort St. John), the majority of seismic events have magnitudes < 2 , meaning that they were difficult to study with the sparse public seismic monitoring networks. Consequently, in early 2020, 13 new broadband seismometers and 2 accelerometers were installed within the KSMMA to enhance the monitoring capabilities of ongoing operations, improve risk assessments and inform mitigation strategies (Figure 1). The installation of such a dense monitoring network aims to enhance the understanding of the generation of felt seismicity due to fluid injection, in particular, the physical processes governing fault (re)activation and arrest, the role of aseismic processes and the management of risk and mitigation strategies related to such events. This is not only important for the operators undertaking hydraulic fracturing experiments in this area, but also for regulators and the general public so that they can improve best practices for safer operations.

This publication is also available, free of charge, as colour digital files in Adobe Acrobat® PDF format from the Geoscience BC website: <http://geosciencebc.com/updates/summary-of-activities/>.

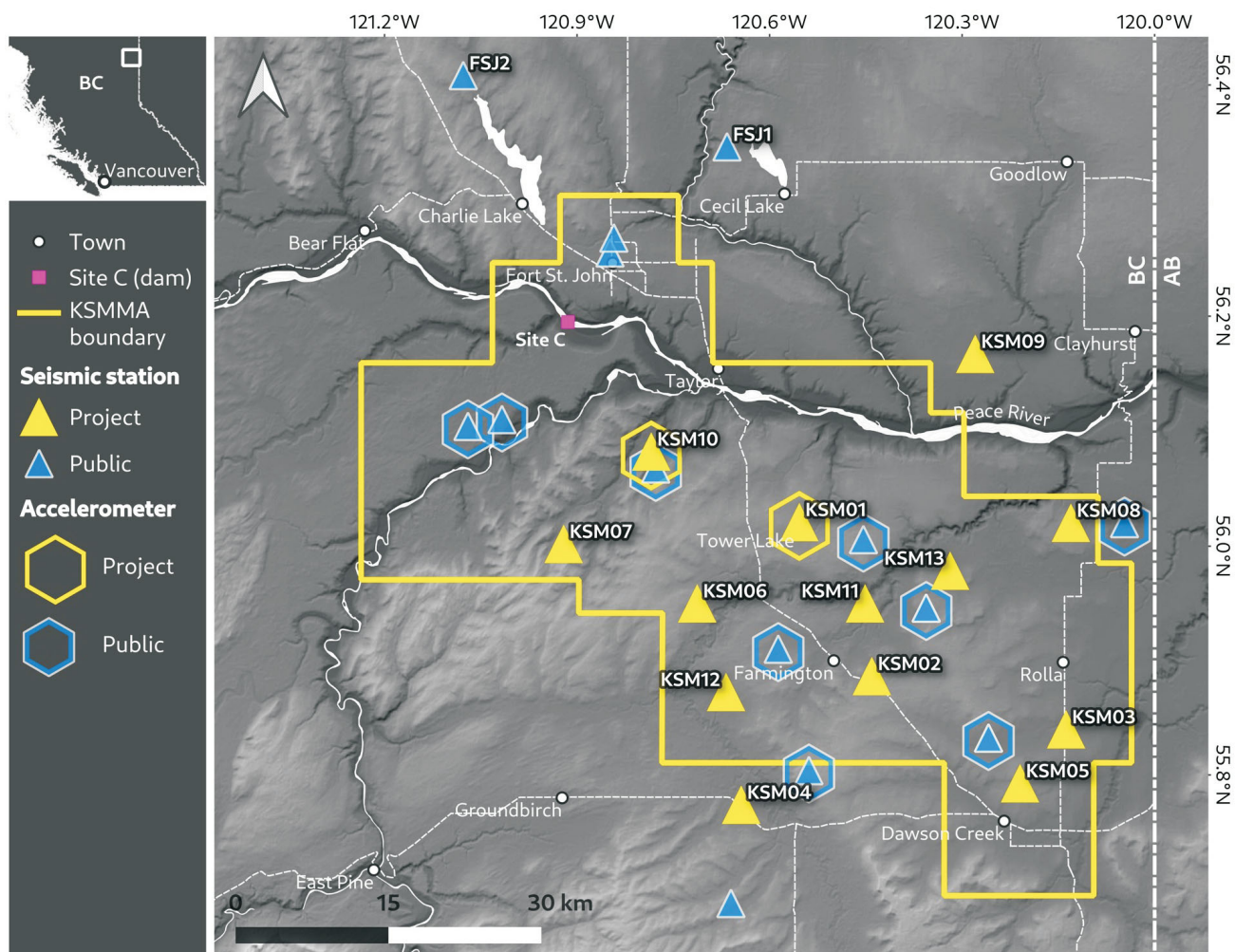


Figure 1. Installed seismic monitoring stations within the Kiskatinaw Seismic Monitoring and Mitigation Area (KSMMA; yellow border), northeastern British Columbia. Yellow stations denote those from a new Earth-System Observing Network–Réseau d’Observation du Système Terrestre (EO) dense array network installed for this project; blue stations are previously installed public stations, managed by Natural Resources Canada (Geological Survey of Canada) and the University of Calgary. Stations FSJ1 and FSJ2 are also part of the EO network but were installed in 2018. Station FSJ1 was decommissioned on August 26, 2020, but is shown for completeness as its data has been used in seismic analyses. Elevation data from Shuttle Radar Topography Mission (U.S. Geological Survey, 2014). WGS 84/ Pseudo-Mercator, World Geodetic System 1984 datum.

Network Design and Installation

With increasing operations within the KSMMA over the past decade, the number of public monitoring stations has also increased. Prior to the installation of this new dense array, nine public sensors maintained by Natural Resources Canada (NRCAN; Geological Survey of Canada) existed within the KSMMA (Figure 1), along with six co-located accelerometers poised to better capture higher levels of ground motion from larger seismic events. Therefore, it was important that the installation of the new dense array complemented the locations of the existing stations. In particular, it was noted that most of the public stations were positioned within a corridor orientated to the northwest, with large gaps in spatial coverage in the northern KSMMA (close to the Site C dam), and in the central area near Tower Lake and in the southwest near Farmington.

Ten broadband seismic stations (Nanometrics Trillium T120 seismometers with Taurus digitizers) were loaned to the University of Calgary for this project by a geothermal research group in South Korea led by T.-S. Kang, S. Kim and J. Rhie. Nanometrics Seismic Monitoring Services (Nanometrics) upgraded the existing firmware on these systems and provided solar power, communication systems and interconnect cables to ensure all systems were fully operational. Furthermore, Nanometrics provided an additional three broadband sensors and two accelerometers (Nanometrics Titan) for the project, as well as undertaking the installation and maintenance of the network. Installation began in January 2020, with four broadband stations and an accelerometer being successfully installed. The remaining stations were installed in March and May 2020. This dense array network adds to two previously installed

stations by the University of Calgary in 2018 in the EON-ROSE (Earth-System Observing Network–Réseau d’Observation du Système Terrestre [EO]) seismic network in this area.

Sensors were installed at existing well sites (Figure 2) through the generous support of four independent companies. The primary aim of the network was to expand monitoring capabilities in the KSMMA, in particular in the northeastern and southwestern parts of the area where prior public monitoring was sparse. However, difficulties relating to the availability of suitable sites (i.e., sites not associated with active well pads and/or having good telecommunication strength) and actual accessibility to sites meant that it was not possible to place sensors in a truly optimum spatial array. In particular, it was not possible to place sensors close to the Site C dam, an area of sparse coverage. For this reason, a decision was made to place two sensors outside of the KSMMA (KSM04 and KSM09, Figure 1) to optimize the aperture of the array, even though these sensors are at a greater distance from ongoing operations than is ideal. Stations KSM01 and KSM10 are centrally located and both have a co-located accelerometer alongside the seismometer. The sites of the accelerometers were chosen due to their proximity to the most recent seismicity in the area, in particular a number of felt events that have occurred close to Tower Lake and Farmington (Figure 3).

Continuous seismic data from the EO network can be downloaded directly from the Incorporated Research Institutions for Seismology (IRIS) website (<https://ds.iris.edu/ds/nodes/dmc/>) following an initial 91 day embargo period reserved for researchers at the University of Calgary and the project partners. Data are released on a 24-hour basis for all stations within the network.

Data Processing

Nanometrics is providing continuous data acquisition, archiving and standard data processing of data from the EO network, as well as incorporating data from the existing public stations in the area. This represents a significant in-kind contribution to this project to produce an accurate and well-maintained catalogue of seismic events during the recording period. The Nanometrics workflow includes event detection, event location analysis and determination of magnitudes, both automatic and through manual inspection by a trained analyst. In March 2020, Nanometrics further supplemented this workflow by deploying AI Analyst advanced processing techniques to augment the automatic processing of data. The full catalogue, including phase pick information and waveform data, as well as the continuous seismic data are provided to researchers so that they can undertake their own analysis of the seismicity.

Firstly, seismic events are detected from the incoming continuous seismic data using a simple short-term average over



Figure 2. a) Example of the footprint of a single seismic monitoring station, showing solar power panels and the top of the short borehole containing the seismometer (Nanometrics Trilium T120). The digitizer (Nanometrics Taurus) and other electronics (e.g., cables, modem, etc.) are housed within the light grey box halfway up the solar panel pole. **b)** Example of the depth of borehole (~30 cm) containing the buried seismometer. Sensors were buried just below the surface to reduce surface noise (e.g., meteorological, traffic, etc.).

long-term average (STA/LTA) triggering algorithm, followed by a separate template-matching algorithm using continuously retrained modules that classify noise from events and remove unwanted signals. Then, the AI Analyst uses the support vector machine (SVM)-learning technique to identify phase arrivals in continuous real-time waveform streams. These phase arrivals are identified by training an SVM model on historical data, as it is a supervised machine-learning approach. By converting the waveforms

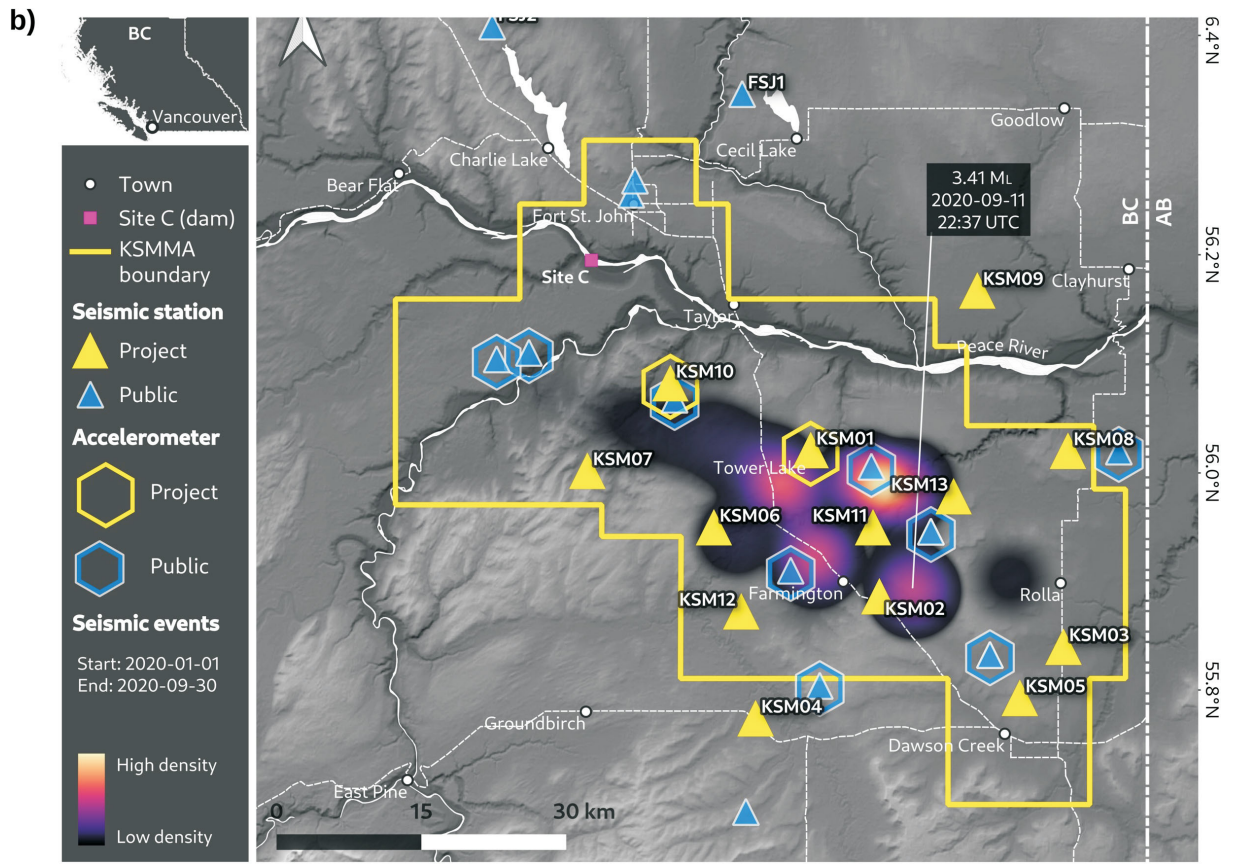
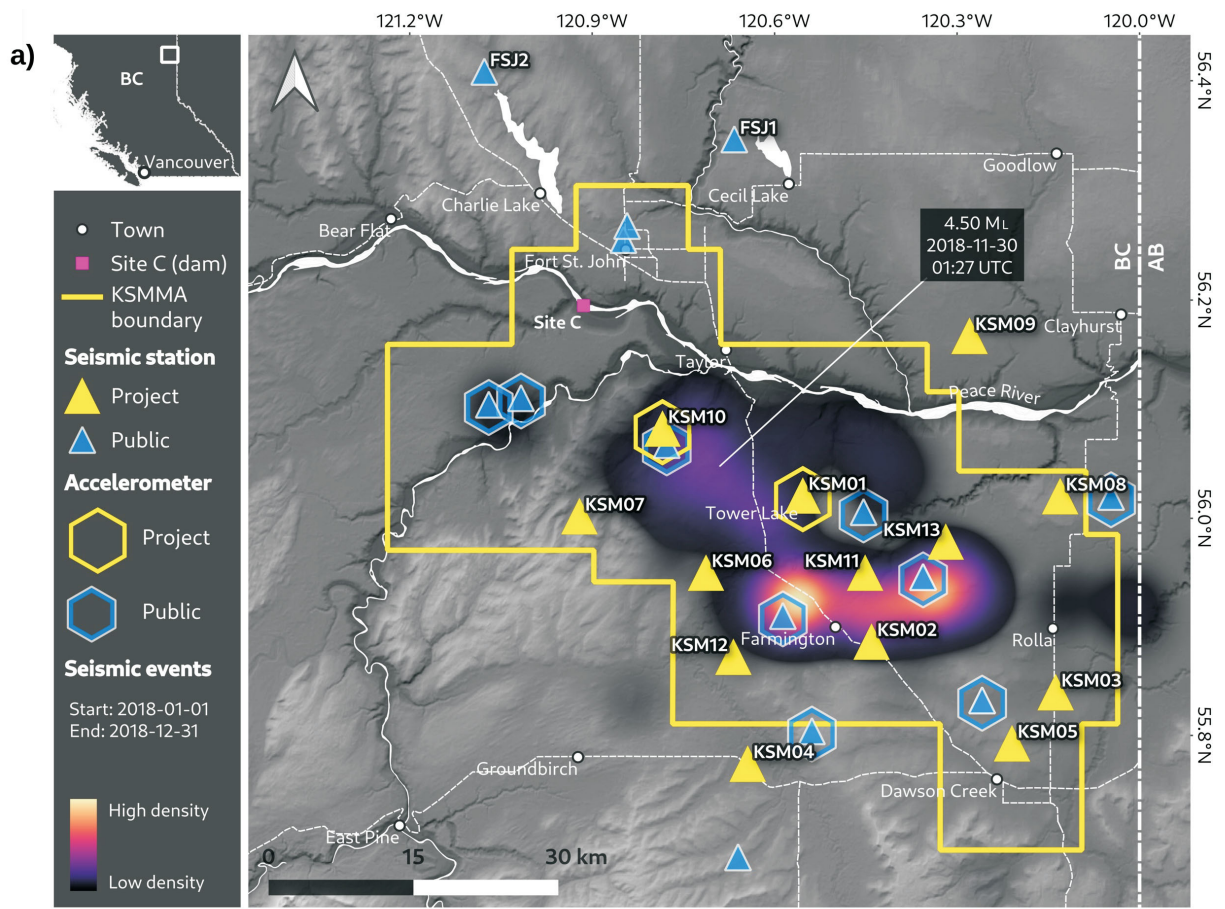


Figure 3. Spatial locations of seismicity concentrations within the Kiskatinaw Seismic Monitoring and Mitigation Area (KSMMA). Higher density of seismic events is indicated by brighter colours; lower density by darker colours; and no seismicity by grey. **a)** Seismic events recorded by Natural Resources Canada between January 1 and December 31, 2018 (data from Visser et al., 2020). Note: although the new dense array was not installed at this time, it is shown on the map for reference. The largest event in 2018, occurring on November 30 north of Tower Lake, is shown (M_L 4.50). **b)** Seismic events recorded on the newly installed Earth-System Observing Network—Réseau d’Observation du Système Terrestre (EO) network (and incorporating data from public stations) from January 22 to September 30, 2020 (data from Nanometrics Seismic Monitoring Services, 2020). The largest magnitude event in 2020, occurring on September 11 east of Farmington, is indicated (M_L 3.41). Stations FSJ1 and FSJ2 are also part of the EO network but were installed in 2018. Station FSJ1 was decommissioned on August 26, 2020, but is shown for completeness as it was used in seismic analysis prior to this. Elevation data from Shuttle Radar Topography Mission (U.S. Geological Survey, 2014). WGS 84/Pseudo-Mercator, World Geodetic System 1984.

into over 250 features using quantities such as time and band-normalized spectrograms, a model is generated that can associate the features with P and S phases (or conversely, with noise). These can then be extracted from real-time waveforms, provided the model is applied to a network of very similar topology and geographic area for which it was trained. Additionally, the phase extraction from real-time data can be used to derive confidence measures in the phases/events detected, as well as to identify and exclude regional events. Once phases have been identified, a beamforming grid-search approach is used to iden-

tify event locations and times based on the highest likelihood P-S separation times observed at all contributing stations.

Event locations are further refined using a double-differencing algorithm (Figure 4) to produce high-precision locations. This uses parameters such as a one-dimensional (1-D) velocity model for the area and cross-correlation specific thresholds, and some parameters relating to event pairing. It reduces errors associated with the velocity model and pick placement by relocating events to minimize a) the travel time differences between co-located event pairs and b) the pick time differences between cross-correlated waveforms from co-located event pairs. A precision estimate is then derived by bootstrapping the input catalogue and quantifying the resultant hypocentre distribution. The 1-D velocity model used has been specially derived for the KSMMA (provided by the BCOGC) based on sonic logs (compressional and shear) and formation tops, and calibrated using events detected on local networks from a number of operators within the KSMMA.

Local magnitudes (M_L) are calculated using a form of the Hutton and Boore (1987) magnitude formula, which was developed for events in southern California that are detected on stations with up to 100 km epicentral distance. This scale is based upon the Wood-Anderson conversion of seismic sensors using the peak S-wave amplitude measurement.

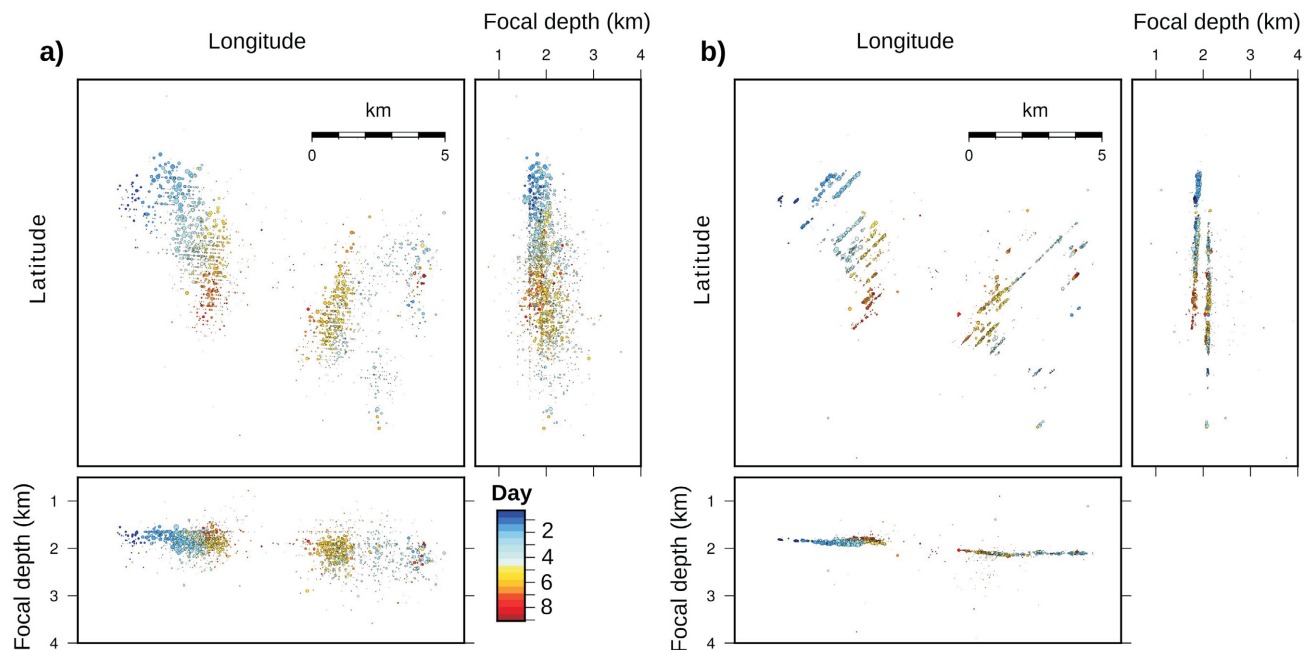


Figure 4. Spatial cluster of 2098 seismic events occurring over ~10 days at the end of March 2020 in part of the Kiskatinaw Seismic Monitoring and Mitigation Area. This example of preprocessing conducted by Nanometrics Seismic Monitoring Services shows the difference between **a)** their calculated standard locations of seismic events and **b)** their calculated high-precision locations of seismic events using a double-differencing algorithm. High-precision locations clearly denote linear features, which appear to correlate temporally with ongoing hydraulic fracturing operations in the area. Latitude and longitude values are not shown in order to preserve the location of this specific seismicity.

Overview of Recorded Seismicity

The first data from the EO network were received on January 22, 2020. At that time four stations had been installed; the remaining stations were installed in the spring. At the time of writing (October 1, 2020), a total of 7216 events had been detected in the KSMMA using the EO network and available public stations, with 7057 events reporting high-precision relocations. All events were automatically detected but have been manually verified by an expert at Nanometrics. Figure 5a (upper) shows the temporal evolution of detected seismicity from January 22 to October 1, 2020, both daily and cumulative. Distinct heightened periods of seismicity can be observed, particularly in February, March, August and September. This reflects ongoing operations in the area during these times. A clear period of quiescence is observed from April until August, representing the unprecedented situation that occurred in 2020 with the lockdown of people, businesses and cities due to the COVID-19 pandemic.

Spatially, seismicity in the KSMMA appears to occur within a band orientated to the northwest-southeast (Figures 3, 5c). Seismicity in 2020 appears to occur within a more spatially distinct region than it did in 2018 (Figure 3b versus 3a), but this may be due to the fact that there have been significantly fewer operations in 2020 due to the COVID-19 pandemic. Interestingly, the largest event in 2018 (M_L 4.50, November 30) occurred to the north of Tower Lake, away from the densest cluster of seismic events (Figure 3a). To date, the largest event of 2020 occurred on September 11 (M_L 3.41) in the southern area of the KSMMA (Figure 3b), but again away from the densest cluster of events. Assuming this seismicity is associated with ongoing hydraulic fracturing operations, this suggests that the largest magnitude events do not necessarily occur near the densest activity. Moreover, given that the largest event in 2020 did not occur in the same cluster as the largest event of 2018, it appears that the occurrence of M_L 3–4+ events is not confined to a single region.

Distinct clusters of seismicity are also seen in focal depth plots (Figure 5c), with the majority of events occurring between 1 and 2 km deep, although a number of smaller events do extend down toward the basement (which lies at an average depth of 4 km across the KSMMA). Target formations for hydraulic fracturing within the KSMMA (e.g., upper and lower Montney Formation) typically sit between 2000 and 2500 m (total vertical depth), suggesting the majority of seismicity occurs within or just above these formations. A deepening of seismicity toward the east likely indicates a deepening of the target formations or target zones in this direction.

As well as detailing the target formations at depth, the spatial evolution of seismicity allows the detailing of fault and

fracture growth in near real-time (Figure 4). High-precision locations (using double-differencing techniques) reveal clear planar features associated with active hydraulic fracturing operations. Figure 4 shows a spatial cluster of 2098 seismic events occurring over ~10 days at the end of March 2020. In Figure 4a, events appear scattered spatially, although there is some degree of order to the events temporally, with the oldest events occurring to the northwest. Following relocation using double-differencing methods (Figure 4b), clear planar features are evident, which appear to ‘grow’ with time toward the southwest. Two distinct populations are identified, which appear to be simultaneously active. The largest planar feature in the southeast is approximately 3 km in length, allowing a better understanding of the extent of ongoing operations in the area, in lieu of having detailed injection data from individual operators.

The installation of the majority of seismic sensors in the EO network in March is clearly evident with the reduction in the minimum detected magnitude at this time (Figure 5a, lower panel). With four stations installed in January (in addition to the public sensors in the area), the minimum detected magnitude was close to M_L 0. In March 2020, this was significantly reduced, with the EO network (when combined with available public stations) now recording some events close to M_L -1. This was partly due to the installation of stations creating a denser network, but also reflects the introduction of the AI Analyst processing tool by Nanometrics, which incorporated machine-learning techniques to further refine M_L for detected events. The current estimated magnitude of completeness (M_c) is 0.074, suggesting that all events larger than this are detected (Figure 5b). This is significantly lower than the estimated M_c of 0.6 that was postulated in the funding proposal to Geoscience BC and is in part due to the optimized network design.

Seismicity directly relating to hydraulic fracturing (operationally induced seismicity) has been shown to have a higher b -value (~2; Maxwell et al., 2009; Wessels et al., 2011), indicating the dominance of many small earthquakes in comparison to large events. In comparison, b -values for natural seismicity in the northern hemisphere sit around 1 (El-Isa and Eaton, 2014). The estimated b -value for events detected in KSMMA, from the EO network and available public station data, is 1.13 (Figure 5b), which suggests that the seismicity has characteristics relating to natural fault systems. Schorlemmer et al. (2005) suggested that the b -value is greatly influenced by the tectonic stress regime, and that a value close to 1.1 is indicative of normal and strike-slip regimes. The KSMMA is strongly influenced by the Fort St. John graben complex, an asymmetrical half graben that has also undergone significant strike-slip and rotational movement upon reactivation of the basement faults in the area (Barclay et al., 1990), with a number

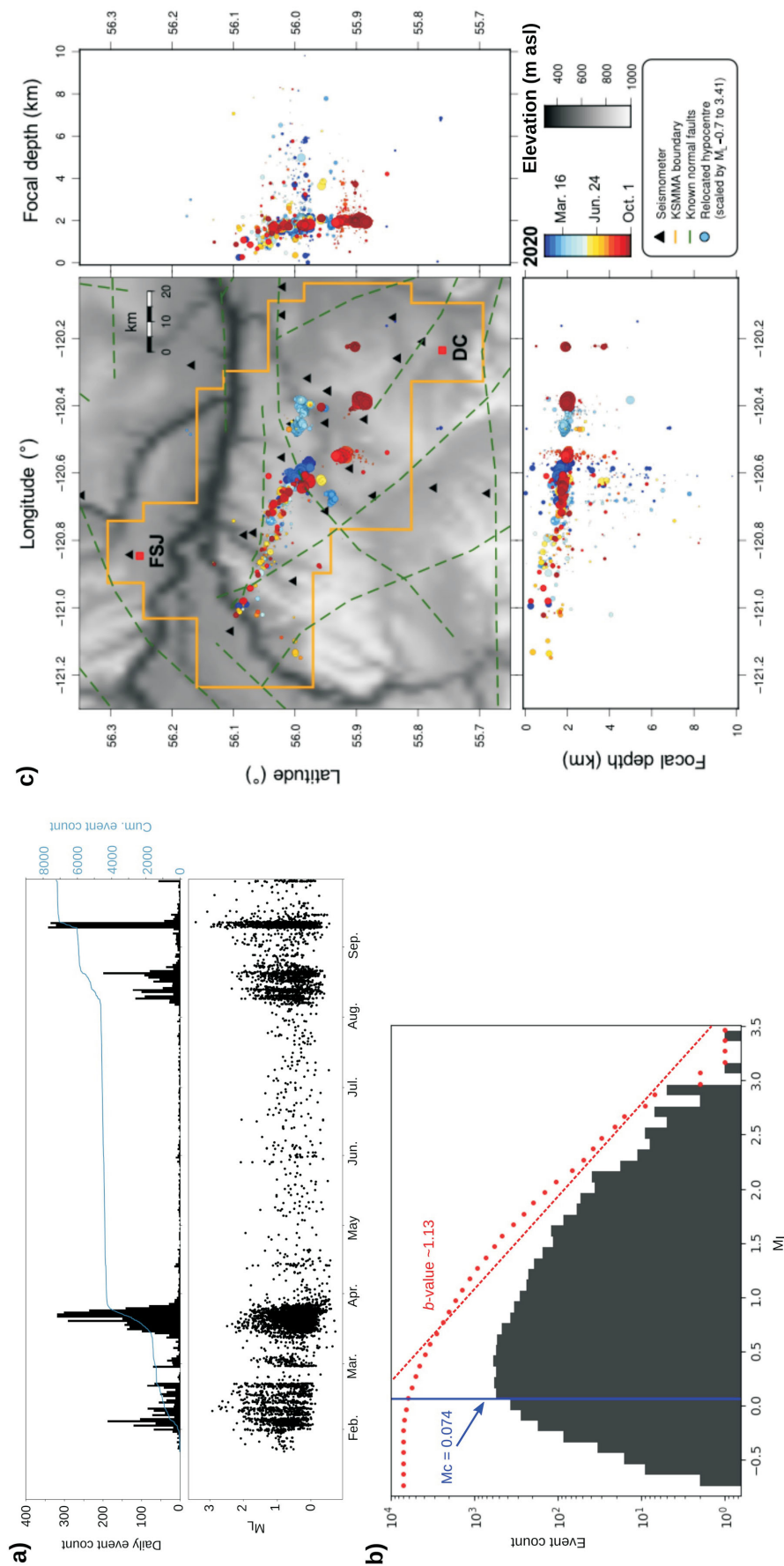


Figure 5. Evolution of seismicity detected since installation of the Earth-System Observing Network-Réseau d'Observation du Système Terrestre (EO) network within the Kiskatinaw Seismic Monitoring and Mitigation Area (KSMMA) from January 22 until October 1, 2020, 7216 events in total. **a)** Time series of events detected. Upper panel denotes event count per day and the cumulative event count through time; lower panel denotes local magnitude (M_L) of each event. Distinct temporal patterns are observed with periods of heightened seismicity in February, March, August and September. These time periods also contain events with seemingly higher magnitude events. **b)** Frequency-magnitude distribution of all events within the catalogue ($n=7216$). The magnitude of completeness (M_c) is estimated to be 0.074, and the estimated b -value is ~ -1.13 . The largest magnitude event in the sequence is M_L 3.41. **c)** Spatial evolution of seismicity, which appears in distinct spatial clusters. The majority of seismic events have a focal depth of 1–2 km. Known normal faults within the KSMMA are shown, taken from Furlong et al., 2020. Abbreviations: Cum., cumulative; DC, Dawson Creek; FSJ, Fort St. John.

of normal faults associated with the extension of the graben falling within the KSMMA (Furlong et al., 2020; Figure 5c).

The largest magnitude event of 2020 at the time of writing (October 1, 2020) occurred on September 11 at 22:37 UTC with an estimated M_L of 3.41, following which operations in the area were shut down in accordance with the BCOGC's traffic light protocol introduced for the KSMMA (BC Oil and Gas Commission, 2018). Due to the COVID-19 pandemic in 2020, operations only restarted in the KSMMA at the beginning of August, following approximately four months of almost total quiescence (Figure 5a). The event on September 11 occurred quickly following this resurgence of activity. A total of 73 precursory events occurred over approximately four hours, with events locating within a small spatial extent (~300 by 150 m). These events are probably directly related to ongoing operations in the area based on the correlation in space and time of events and injection. Events within this precursory sequence had magnitudes between M_L 0.2 and 2.6, and were all located at depths of approximately 2.05 km. The mainshock was located at a similar depth of 2.01 km.

Ongoing Research

Seismic data is analyzed in near real-time by Nanometrics to provide an accurate and up-to-date catalogue of seismicity. Using this as a base, the University of Calgary, in collaboration with other institutions, is undertaking further research into the seismic sequences that are occurring within the KSMMA, in particular, the characteristics of the source of the events, spatio-temporal clustering of events, and fault and fracture dynamics at depth.

Understanding the source characteristics of an earthquake is fundamental to better discerning the physics behind source rupture processes and the kinematic behaviour of the source, and consequently understanding why seismic activity manifested in the first instance (e.g., Kanamori and Brodsky, 2004; Abercrombie, 2015). This is important for the determination of hazards in the area. Characterization of an earthquake source in terms of the deformation the rupture produces is fundamental to understand the evolving stress field and growing fracture network within a given environment (e.g., Eyre and van der Baan, 2015). One common method for calculating this is the moment tensor inversion (MTI), which aims to calculate the magnitude and orientation of fracture planes often based on body-wave polarities, amplitude ratios or waveform inversions.

A fully nonlinear Bayesian centroid moment tensor (CMT) inversion, based on the Bayesian earthquake analysis tool (BEAT; Vasyura-Bathke et al., 2020) software, was carried out for the September 11, 2020, M_L 3.41 event (Figure 6). Data from 12 stations were processed in units of velocity and a 3rd order Butterworth filter between 0.07 and 0.2 hertz

was applied after instrument-response removal. Data included waveforms from an array in the Dawson-Septimus area (Roth et al., 2020). After rotation into radial, transverse and vertical components, only components with a pulse-like waveform were retained. Green's functions were computed with QSEIS software (Wang, 1999) for a 1-D velocity model that is representative of the Western Canada Sedimentary Basin (Wang et al., 2016). The inversion applies a lune parametrization (Tape and Tape, 2015) and includes a Bayesian implementation of the cut-and-paste (CAP) algorithm (Zhao and Helmberger, 1994) to account for potential 3-D velocity structure that is not included in the 1-D velocity model. Whereas the original CAP algorithm infers optimal time shifts, the Bayesian method fully accounts for uncertainty of these time shifts within a window of ± 3 s.

The CMT results show a focal mechanism dominated by a strike-slip mechanism (Figure 6a). The fault strikes at 246° with uncertainty between 245 and 249° . The auxiliary plane strikes at 86° with uncertainty between 82 and 87° . The centroid is located at 2.6 km depth with low uncertainty. The centroid epicentre is shifted 0.4 km west and 0.5 km north compared to the catalogue location. The mechanism (Figure 6a) is predominantly a double-couple solution (72.7–85.4%). However, 2.4–9.3% of the source is explained by an isotropic component and 6.4–22.4% by a compensated linear vector dipole (CLVD). Such isotropic and CLVD components are not uncommon and are typically ascribed to theory errors in the inversion. For example, the fault plane may not be perfectly planar, and Green's functions may include errors. It is also noted that CMT decomposition is intrinsically based on assumptions and it is more rigorous to consider these source trade-offs with the lune diagram (Figure 7), which illustrates the uncertainty in terms of the colour scale. The results are consistent with other studies of source mechanisms within the KSMMA, which suggest mechanisms are dominated by strike-slip faulting, with some evidence of thrust faulting (Wang et al., 2018; Babaie Mahani et al., 2020).

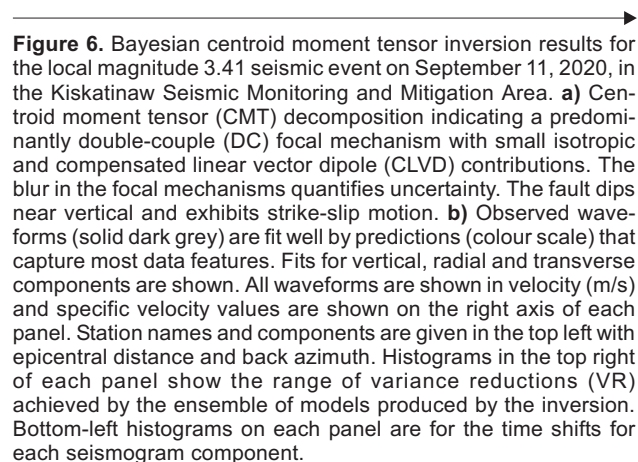
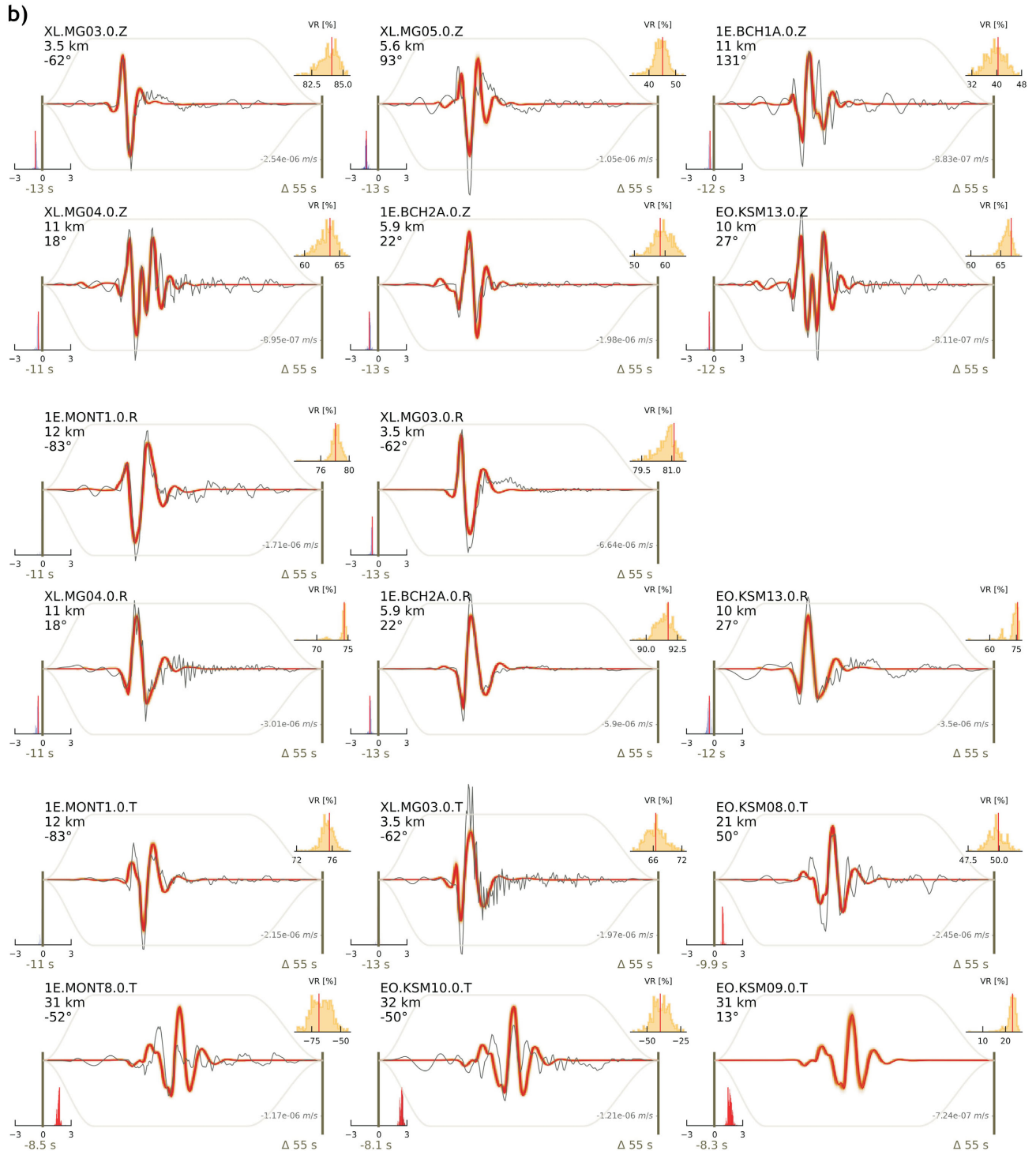
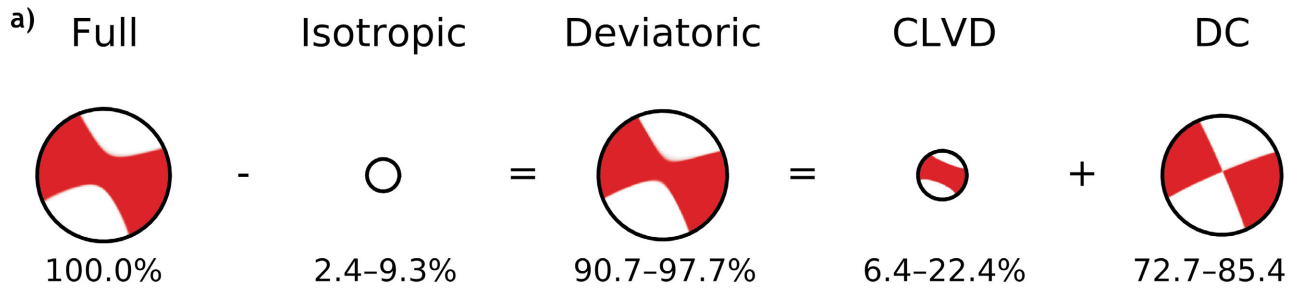


Figure 6. Bayesian centroid moment tensor inversion results for the local magnitude 3.41 seismic event on September 11, 2020, in the Kiskatinaw Seismic Monitoring and Mitigation Area. **a)** Centroid moment tensor (CMT) decomposition indicating a predominantly double-couple (DC) focal mechanism with small isotropic and compensated linear vector dipole (CLVD) contributions. The blur in the focal mechanisms quantifies uncertainty. The fault dips near vertical and exhibits strike-slip motion. **b)** Observed waveforms (solid dark grey) are fit well by predictions (colour scale) that capture most data features. Fits for vertical, radial and transverse components are shown. All waveforms are shown in velocity (m/s) and specific velocity values are shown on the right axis of each panel. Station names and components are given in the top left with epicentral distance and back azimuth. Histograms in the top right of each panel show the range of variance reductions (VR) achieved by the ensemble of models produced by the inversion. Bottom-left histograms on each panel are for the time shifts for each seismogram component.



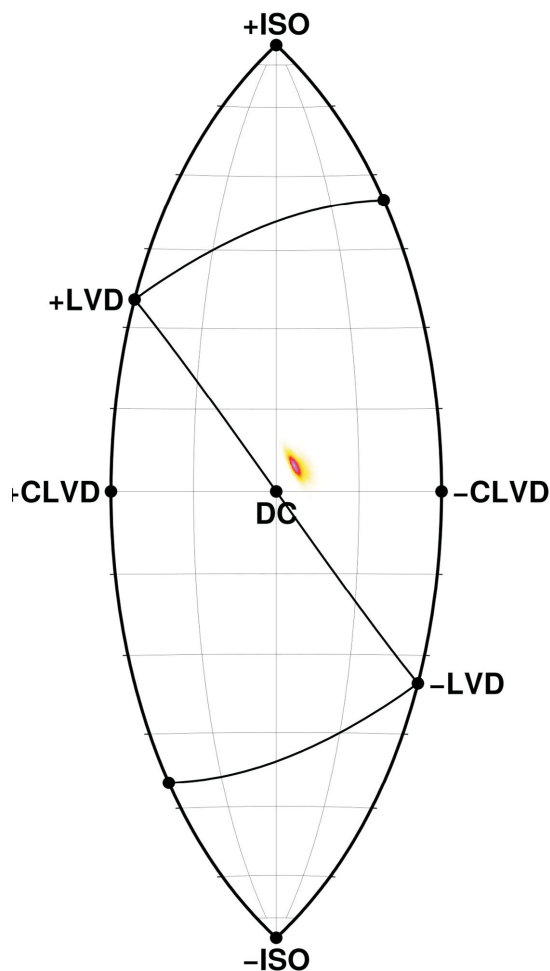


Figure 7. Bayesian centroid moment tensor (CMT) inversion results for the local magnitude 3.41 seismic event on September 11, 2020. The lune representation of the CMT more clearly shows that the event can be predominantly explained by slip on a planar fault, where the colour scale presents the probability. Lighter colours indicate low probability; darker colours indicate high probability. Abbreviations: CLVD, compensated linear vector dipole; DC, double couple; ISO, isotropic; LVD, linear vector dipole.

Observed waveforms and prediction fits, CAP time shifts and variance reduction are shown in Figure 6b. Note that agreements are excellent overall but some of the largest amplitudes are not fit well. The CAP time shifts required are negative for vertical and radial components and notably positive or neutral for the transverse component. This difference may suggest some degree of crustal anisotropy.

Since CMT estimates disagree with catalogue values, the hypocentre depth and magnitude were recalculated independently using seismic phase picks provided in the catalogue. A focal depth of ~ 2.75 km was calculated, which closely agrees with the centroid depth but is deeper than the hypocentre depth of ~ 2 km in the catalogue. Similarly, a smaller magnitude of $\sim M_L 3.1$ (compared to $M_L 3.41$) was calculated. Both of these estimates agree with the CMT inversion. The discrepancy in the calculated and the original magnitude is due to the use of a different formula for calcu-

lation—a form of the Richter (1935) magnitude formula that has been modified to better reflect local attenuation characteristics of the KSMMA (Babaie Mahani and Kao, 2020) was used. In line with calculations done by NRCan, the M_L was calculated using the maximum amplitude from the vertical component, simulated on a Wood-Anderson (WA) seismometer, rather than the horizontal component, which is more common elsewhere. Plans are being made to extend the work to include events prior to this mainshock to understand the evolution of stress with time.

The year 2020 was unusual due to the COVID-19 pandemic, which caused the shutdown of many businesses and severely restricted the movement of people. A related reduction in ground motion has been accurately measured by a drop in seismic noise worldwide (e.g., Lecocq et al., 2020), which is also evidenced in the KSMMA. Over the approximately four months of quiescence, when operations within KSMMA ceased due to government regulations (April to August, Figure 5a), only 389 events were detected using the EO network and available public stations in the area. For comparison, 344 events were detected on the EO network over a single week, from February 8 to 15, when operations were in full flow. The seismicity that occurred during the quiescence is being investigated: Is it latent seismicity left over from operations in wells in the KSMMA? If so, is this from very recent operations or is it from more long-term operations? Or does it represent a natural seismicity that is now evident in the area due to changes to stress brought about by anthropogenic activity in the area? The unprecedented period of quiet allows the authors to better constrain the seismicity, since it cannot have been induced by ongoing operations in the area.

Preliminary investigations into spatio-temporal clustering of seismicity and interevent triggering within the KSMMA are being undertaken. There appears to be some evidence of interevent triggering, but correlation with injection parameters for individual wells is still required and the degree to which this influences spatio-temporal clustering remains unclear. There is also an interest in better understanding local site effects for hazard analysis, in particular, investigating spectral peaks due to resonance effects and their possible seasonal variation and amplification of seismic waves within the KSMMA. This may lead to a better understanding of why the report rate of seismic events varies spatially across the KSMMA, and why a number of residents are reporting feeling strong shaking with only very moderate magnitude events ($M_L < 2$). Monahan et al. (2019) concluded that site amplification conditions within the KSMMA are varied, with Site Class D conditions (high amplification of seismic ground motions) being widespread. Analysis of the ambient seismic noise field, and in particular the horizontal to vertical spectral ratio (HVSF), will allow the determination of the fundamental site response frequency at different sites within KSMMA. Both of these

studies aim to better constrain the hazard from ongoing seismicity within the KSMMA, detecting ‘weak’ zones where seismicity is prevalent and could potentially cause alarm for the public due to amplification of the seismic wavefield.

High-precision locations of events suggest distinct planar features that develop in regions are related to ongoing hydraulic fracturing operations (e.g., Figure 4). Therefore, an analysis is being undertaken to better understand the spatio-temporal evolution of the rupture process of such planar features, using finite-fault source inversions and Bayesian analysis to better constrain the uncertainties associated with such analysis. It is hoped that this will provide a better understanding of fault nucleation, propagation and arrest, which is essential knowledge for operators and regulators.

Finally, the detailed monitoring within the KSMMA may allow the authors to better constrain a long-standing problem linked to induced seismicity: Are there diagnostic differences in the characteristics of seismicity induced by hydraulic fracturing and seismicity induced from wastewater disposal? Are the source mechanisms and rupture processes similar or different? In Canada, the majority of induced seismicity is associated with hydraulic fracturing (e.g., Rivard, 2014; Atkinson, 2016), however, in some areas of the United States seismicity is strongly associated with wastewater disposal (e.g., Ellsworth, 2013). Within the KSMMA, there are both unconventional reservoirs and wastewater disposal wells, which provides a unique opportunity to study both in detail. Currently a spatio-temporal analysis of events associated with both types of wells is being undertaken, as well as comparisons of magnitudes and source parameters, including MTI and stress changes, to better understand whether it is possible to discriminate between these two types of seismicity, and if so, learn about each of their fundamental characteristics. The objective is to gain a better understanding of the characteristic seismicity of each of these types of operations, which will enable the characterization of incoming seismicity in near real time. It will also be possible to provide insights on seismicity generation and evolution under different stress conditions to all those involved in the oil and gas industry and regulatory bodies.

Conclusions

In January 2020, the installation of a new dense seismic monitoring network began within the Kiskatinaw Seismic Monitoring and Mitigation Area (KSMMA), to better understand the relationship between ongoing hydraulic fracturing and wastewater injection operations and seismicity, in particular seismicity which is unexpected (either in terms of its location or magnitude), and seismicity that is felt by the general population. With the installation of a dense ar-

ray network, the hope is to better capture seismicity in the KSMMA at smaller magnitudes, and thereby generate a more complete catalogue of events. This catalogue will be used to better characterize the faulting and fracture mechanisms within this area, the site amplification effects and the spatial and temporal relationship between seismicity and operations, which will lead to a better understanding of the area’s susceptibility to larger magnitude events. This can all aid regulatory practices and promote safer operations by the oil and gas industry within British Columbia.

The unique nature of this project means close collaboration with partners in both industry and academia to enhance the likelihood of success. By providing an evolving event catalogue (event timings, locations, magnitudes), Nanometrics Seismic Monitoring Services are significantly helping to accelerate the research within the KSMMA. To date, over 7200 events have been detected within the KSMMA using the new network and available public station networks, down to local magnitudes of -1 . The installation of the new network has significantly reduced the magnitude of completeness of events detected in this area, meaning that a more complete picture of ongoing seismicity within the KSMMA has been achieved. Events appear very temporally and spatially clustered, probably related to ongoing operations in the area. Spatially, seismicity is following a similar pattern to previous years, where events cluster within a central band extending northwest to southeast. Clustering of events at depths around 2 km indicates a likely correlation between hydraulic fracturing and seismicity, as this is the average target depth of geological formations within the KSMMA. Having high-resolution locations may allow the authors to better constrain this relationship, and in particular the relationship between individual stages of operations and the temporal nature/spatial nature/magnitude of seismicity. The largest event to have occurred so far in 2020 (September 11) suggests a mechanism dominated by strike-slip movement. Using the generated seismic catalogue from the new network and available public stations, the analysis is being extended to better understand the processes at the sources of seismicity within the KSMMA and provide better constraints on faults and fractures in this area, especially their activation and development in relation to ongoing operations.

Acknowledgments

The authors thank Geoscience BC for funding this project. They also acknowledge the industry partners whose collaboration enabled the installation of this network. They would like to thank ARC Resources Ltd., Canadian Natural Resources Limited and the Natural Sciences and Engineering Research Council of Canada for providing further funding for this project. Nanometrics Seismic Monitoring Services is gratefully acknowledged for their contribution to this project, including the installation and maintenance of

stations, and near real-time analysis of incoming seismicity. The authors would like to thank those at the Incorporated Research Institutions for Seismology (IRIS) for hosting the data and facilitating collaboration. They would especially like to thank J. Hogan at Nanometrics, who facilitated the successful upload of data to IRIS, and A. Baig at Nanometrics for careful review of this manuscript. Also, thanks go to H. Vasyura-Bathke at the University of Potsdam/GFZ German Research Centre for Geosciences for their support in determining centroid moment tensor parameters. The authors are grateful for access to data from the XL network (https://www.fdsn.org/networks/detail/XL_2017/) for the moment tensor inversion. Finally, they would like to thank S. Venables and M. Gaucher at the BC Oil and Gas Commission for their continued support and invaluable knowledge that the authors have often called upon, and C. Furlong and Geoscience BC for assisting with the review process of this article.

References

- Abercrombie, R.E. (2015): Investigating uncertainties in empirical Green's function analysis of earthquake source parameters; *Journal of Geophysical Research: Solid Earth*, v. 120, issue 6, p. 4263–4277, URL <<https://doi.org/10.1002/2015JB011984>>.
- Atkinson, G.M., Eaton, D.W., Ghofrani, H., Walker, D., Cheadle, B., Schultz, R., Shcherbakov, R., Tiampo, K., Gu, J., Harrington, R.M., Liu, Y., van der Baan, M. and Kao, H. (2016): Hydraulic fracturing and seismicity in the Western Canada Sedimentary Basin; *Seismological Research Letters*, v. 87, no. 3, p. 631–647, URL <<https://doi.org/10.1785/0220150263>>.
- Babaie Mahani, A. and Kao, H. (2020): Determination of local magnitude for induced earthquakes in the Western Canada Sedimentary Basin: an update; *CSEG Recorder*, v. 45, no. 2, URL <<https://csegrecorder.com/articles/view/determination-of-local-magnitude-for-induced-earthquakes-in-the-wcsb>> [October 2020].
- Babaie Mahani, A., Esfahani, F., Kao, H., Gaucher, M., Hayes, M., Visser, R. and Venables, S. (2020): A systematic study of earthquake source mechanism and regional stress field in the southern Montney unconventional play of northeast British Columbia, Canada; *Seismological Research Letters*, v. 91, no. 1, p. 195–206, URL <<https://doi.org/10.1785/022019-0230>>.
- Barclay, J.E., Krause, F.F., Campbell, R.I. and Utting, J. (1990): Dynamic casting and growth faulting: Dawson Creek graben complex, Carboniferous–Permian Peace River embayment, western Canada; *Bulletin of Canadian Petroleum Geology*, v. 38, issue 1, p. 115–145, URL <https://pubs.geoscienceworld.org/cspg/bcpg/article/38A/1/115/582791/Dynamic-casting-and-growth-faulting-Dawson-Creek?casa_token=3fNc9UphmkkAAAAA:-16XUfhwg-2u4WaQ6JxM8unvNr7TbyR5SkyQXBmqeMtiKH8OZTb0xzEQuDEyey60HDIRIQ5o> [November 2020].
- BC Oil and Gas Commission (2018): Order 18-90-001 (amendment #1) – Kiskatinaw Seismic Monitoring and Mitigation Area Special Project Order; BC Oil and Gas Commission, URL <<https://www.bcogc.ca/files/reports/Technical-Reports/Kiskatinaw-Seismic-Monitoring-and-Mitigation-Area-KSMMA-Special-Project-Order-18-90-001-Amendment-1.pdf>> [October 2020].
- El-Isa, Z.H. and Eaton, D.W. (2014): Spatiotemporal variations in the *b*-value of earthquake magnitude–frequency distributions: classification and causes; *Tectonophysics*, v. 615, p. 1–11, URL <<https://doi.org/10.1016/j.tecto.2013.12.001>>.
- Ellsworth, W.L. (2013): Injection-induced earthquakes; *Science*, v. 341, issue 6142, art. 1225942, URL <<https://doi.org/10.1126/science.1225942>>.
- Eyre, T.S. and van der Baan, M. (2015): Overview of moment-tensor inversion of microseismic events; *The Leading Edge*, v. 34, no. 8, p. 882–888, URL <<https://doi.org/10.1190/tle-34080882.1>>.
- Furlong, C.M., Gingras, M.K. and Zonneveld, J.P. (2020): High-resolution sequence stratigraphy of the Middle Triassic Sunset Prairie Formation, Western Canada Sedimentary Basin, north-eastern British Columbia; *The Depositional Record*, v. 6, issue 2, p. 343–408, URL <<https://doi.org/10.1002/dep2.107>>.
- Hutton, L.K. and Boore, D.M. (1987): The ML scale in southern California; *Bulletin of the Seismological Society of America*, v. 77, no. 6, p. 2074–2094, URL <https://pubs.geoscienceworld.org/ssa/bssa/article/77/6/2074/119025?casa_token=PI7rujdIrZwAAAAA:-GNMZJu9tTvReL9QJWdi7EU01HkyrRhGoRaj56aieX2LgzEja_3CSX6hv6L5INaifgMw> [October 2020].
- Kanamori, H. and Brodsky, E.E. (2004): The physics of earthquakes; *Reports on Progress in Physics*, v. 67, no. 8, p. 1429–1496, URL <<https://doi.org/10.1088/0034-4885/67/8/R03>>.
- Lecocq, T., Hicks, S.P., Van Noten, K., van Wijk, K., Koelemeijer, P., De Plaen, R.S.M., Massin, F., Hillers, G., Anthony, R.E., Apoloner, M.-T., Arroyo-Solorzano, M., Assink, J.D., Buyukakpinar, P., Cannata, A., Cannavo, F., Carrasco, S., Caudron, C., Chaves, E.J., Cornwell, D.G., Craig, D., et al. (2020): Global quieting of high-frequency seismic noise due to COVID-19 pandemic lockdown measures; *Science*, v. 369, issue 6509, p. 1338–1343, URL <<https://doi.org/10.1126/science.abd2438>>.
- Maxwell, S.C., Jones, M., Parker, R., Miong, S., Leaney, S., Dorval, D., D'Amico, D., Logel, J., Andersen, E. and Hammermaster, K. (2009): Fault activation during hydraulic fracturing; *Society of Exploration Geophysicists, SEG 2009 Annual Meeting*, October 25–30, 2009, Houston, Texas, Technical Program Expanded Abstracts, p. 1552–1556, URL <<https://doi.org/10.1190/1.3255145>>.
- Monahan, P.A., Hayes, B.J., Perra, M., Mykula, Y., Clarke, J., Galamboos, B., Griffiths, D., Bayarsaikhan, O. and Oki, U. (2019): Amplification of seismic ground motion in the Fort. St. John–Dawson Creek area, northeastern British Columbia (NTS 093P, 094A); *in Geoscience BC Summary of Activities 2019: Energy and Water*, Geoscience BC, Report 2020-02, p. 1–12, URL <http://www.geosciencebc.com/i/pdf/SummaryofActivities2019/EW/Project%202018-052_EW_SOA2019.pdf> [October 2020].
- Nanometrics Seismic Monitoring Services (2020): Athena web portal; Nanometrics Seismic Monitoring Services, URL <<https://www.nanometrics.ca/products/software/athena>> [October 2020].
- Richter, C.F. (1935): An instrumental earthquake magnitude scale; *Bulletin of the Seismological Society of America*, v. 25, no. 1, p. 1–32, URL <https://pubs.geoscienceworld.org/ssa/bssa/article/25/1/1/115102?casa_token=Z56vuucvly>.

- UAAAAA:uWJSrF7dP-J9x-ZJiiKMKV5TY0QZy-ayaVS6QmYEkF82cNy9Y3f4tRxxX4estOSXZ1ePiM> [October 2020].
- Rivard, C., Lavoie, D., Lefebvre, R., Séjourné, S., Lamontagne, C. and Duchesne, M. (2014): An overview of Canadian shale gas production and environmental concerns; *International Journal of Coal Geology*, v. 126, p. 64–76, URL <<https://doi.org/10.1016/j.coal.2013.12.004>>.
- Roth, M.P., Verdecchia, A., Harrington, R.M. and Liu, Y. (2020): High-resolution imaging of hydraulic-fracturing induced earthquake clusters in the Dawson-Septimus area, northeast British Columbia, Canada; *Seismological Research Letters*, v. 91, no. 5, p. 2744–2756, URL <<https://doi.org/10.1785/0220200086>>.
- Schorlemmer, D., Wiemer, S. and Wyss, M. (2005): Variations in earthquake-size distribution across different stress regimes; *Nature*, v. 437, p. 539–542, URL <<https://doi.org/10.1038/nature04094>>.
- Tape, W. and Tape, C. (2015): A uniform parametrization of moment tensors; *Geophysical Journal International*, v. 202, issue 3, p. 2074–2081, URL <<https://doi.org/10.1093/gji/ggv262>>.
- U.S. Geological Survey (2014): Shuttle Radar Topography Mission, digital topographic data; U.S. Geological Survey, 30 m cell, zipped hgt format, URL <<http://dds.cr.usgs.gov/srtm/>> [October 2020].
- Vasyura-Bathke, H., Dettmer, J., Steinberg, A., Heimann, S., Isken, M.P., Zielke, O., Mai, P.M., Sudhaus, H. and Jónsson, S. (2020): The Bayesian earthquake analysis tool; *Seismological Research Letters*, v. 91, no. 2A, p. 1003–1018, URL <<https://doi.org/10.1785/0220190075>>.
- Visser, R., Kao, H., Smith, B., Goerzen, C., Kontou, B., Dokht, R.M.H., Hutchinson, J., Tan, F. and Babaie Mahani, A. (2020): A comprehensive earthquake catalogue for the Fort St. John – Dawson Creek region, British Columbia, 2017–2018; Geological Survey of Canada, Open File 8718, 20 p., URL <<https://doi.org/10.4095/326015>>.
- Wang, R. (1999): A simple orthonormalization method for stable and efficient computation of Green’s functions; *Bulletin of the Seismological Society of America*, v. 89, no. 3, p. 733–741, URL <https://pubs.geoscience-world.org/ssa/bssa/article/89/3/733/120414?casa_token=thLuvQpSH9MAAAAAA:-CAzeIbpJr9NwXs4iLEqc1t20hNqWO1EVDad8GWCWtNCMXeqj8O2Ldetl50c1_eR_523Bw8> [October 2020].
- Wang, R., Gu, Y.J., Schultz, R. and Chen, Y. (2018): Faults and non-double-couple components for induced earthquakes; *Geophysical Research Letters*, v. 45, issue 17, p. 8966–8975, <<https://doi.org/10.1029/2018GL079027>>.
- Wang, R., Gu, Y.J., Schultz, R., Kim, A. and Atkinson, G. (2016): Source analysis of a potential hydraulic-fracturing-induced earthquake near Fox Creek, Alberta; *Geophysical Research Letters*, v. 43, issue 2, p. 564–573, URL <<https://doi.org/10.1002/2015GL066917>>.
- Wessels, S., Kratz, M. and De La Pena, A. (2011): Identifying fault activation during hydraulic stimulation in the Barnett Shale: source mechanisms, *b* values, and energy release analyses of microseismicity; Society of Exploration Geophysicists, SEG 2011 Annual Meeting, September 18–23, 2011, San Antonio, Texas, Technical Program Expanded Abstracts, p. 1463–1467, URL <<https://doi.org/10.1190/1.3627478>>.
- Zhao, L.S. and Helmberger, D.V. (1994): Source estimation from broadband regional seismograms; *Bulletin of the Seismological Society of America*, v. 84, no. 1, p. 91–104, URL <https://pubs.geoscienceworld.org/ssa/bssa/article/84/1/91/1102552?casa_token=SGrBfXFt1-WQAAAAA:wc0w90lgm_hiViAtij3P90ePfluK85nzL8LQQPvx0B7Gi0Y8TMXWImxDYW3VGGDQYqf5w> [October 2020].

